Medical Oncology (2019) 36:82
https://doi.org/10.1007/s12032-019-1303-z

ORIGINAL PAPER

EMT-related protein expression in polyploid giant cancer cells and their daughter cells with different passages after triptolide treatment

Xinlu Wang[1] · Minying Zheng[1] · Fei Fei[1] · Chunyuan Li[1] · Jiaxing Du[1,2] · Kai Liu[1,3] · Yuwei Li[4] · Shiwu Zhang[1]

Received: 4 June 2019 / Accepted: 4 August 2019 / Published online: 12 August 2019

Abstract

Our previous work has demonstrated that paclitaxel can induce the formation of polyploid giant cancer cells (PGCCs) and inhibit tumor growth by reprogramming ovarian cancer epithelial cells to a benign fibroblastic state via epithelial–mesenchymal transition. Here, triptolide (TPL) was used to treat the breast and ovarian cancer lines. The morphologic characteristics and EMT-related protein expression were studied in different generation of cancer cells after TPL treatment. When BT-549 and HEY cells reached 80–90% confluence, TPL was added to BT-549 for 48 h and HEY for 9 h at a concentration of 40 ng/ml. Scattered PGCCs survived from TPL treatment and generated daughter cells, and then were cultured in medium without TPL for at least ten generation. Western blot analysis and immunocytochemical staining were performed to detect the expression levels and subcellular location of EMT-related proteins in control cells and different generation of TPL-induced PGCCs with daughter cells. Furthermore, wound-healing, transwell, cell counting kit-8, and MTT assay were used to compare the alternation of migration, invasion, and proliferation among control cells and different generation of TPL-induced PGCCs with daughter cells. Scattered PGCCs survived from the treatment of TPL and produced small-sized daughter cells 20–30 days after treatment. Compared to the control cells, the first generation of TPL-induced PGCCs with their daughter cells differentially expressed EMT-related proteins including fibronectin, E-cadherin, vimentin, and Twist, and had lower migration, invasion, and proliferation abilities. The abilities of migration, invasion, and proliferation of TPL-induced PGCCs with their daughter cells gradually enhanced as the passages increasing, and markedly exceeded the control cells in the tenth generation. TPL-induced PGCCs with their daughter cells gradually obtain the abilities of invasion and metastasis in vitro as the number of passage increasing, which can be used to mimick the cancer cells subjected to anti-cancer drugs in vivo and may provide some new insights to explore the mechanism of cancer invasion, metastasis and relapse after chemotherapy.

Keywords Triptolide · Polyploid giant cancer cells · Epithelial–mesenchymal transition

✉ Shiwu Zhang
zhangshiwu666@aliyun.com

Xinlu Wang
wangxinlu1007@163.com

Minying Zheng
zhengminying1004@163.com

Fei Fei
1120160483@mail.nankai.edu.cn

Chunyuan Li
2120161210@mail.nankai.edu

Jiaxing Du
djx13131313@126.com

Kai Liu
Liukaikai1661@163.com

Yuwei Li
liyuwei66@163.com

[1] Department of Pathology, Tianjin Union Medical Center, Tianjin 300121, People's Republic of China

[2] Tianjin University of Traditional Chinese Medicine, Tianjin 300193, People's Republic of China

[3] Graduate School of Tianjin Medical University, Tianjin 300070, People's Republic of China

[4] Departments of Colorectal Surgery, Tianjin Union Medical Center, Tianjin 300121, People's Republic of China

Introduction

Breast cancer is the third most frequently diagnosed cancer and the leading cause of cancer-related deaths in women worldwide, and 2.1 million new female breast cancer cases occured in the world in 2018 [1]. Ovarian cancer has the highest mortality among gynecological malignant tumors, with a 30% 5-year survival rate [2, 3]. Cancer metastasis and relapse are mostly responsible for the mortality associated with breast and ovarian cancers, even though patients undergo surgery, chemotherapy, and radiation therapy [3–5]. Our previous works reported that polyploid giant cancer cells (PGCCs) are induced by cobalt chloride ($CoCl_2$) [6] and paclitaxel [7] in ovarian [8, 9], breast [7, 10], and colorectal cancers [11, 12]. As a special subpopulation of cancer cells, PGCCs are at least three times larger in size or have more than three irregular nuclei compared with normal cancer cells, with cancer stem-like properties to generate daughter cells via asymmetric cell division [6]. The daughter cells derived from PGCCs showed stronger migratory and invasive abilities than the control cells by upregulation of hypoxia-inducible factor (HIF)-1 alpha and its known target stanniocalcin 1, stem cell-regulating factors, and epithelial–mesenchymal transition (EMT) -related proteins [13]. Furthermore, we confirmed that PGCCs had low expression of cytokeratin and E-cadherin and high expression of fibronectin, vimentin, snail, and slug in ovarian cancer [14], and Twist, slug, and snail in colorectal cancer [12]. Daughter cells generated from PGCCs by $CoCl_2$ had strong ability of migration and invasion. PGCCs induced by paclitaxel and their daughter cells also underwent a markedly morphologic transition from the epithelial to mesenchymal phenotype. However, the proliferation and invasion ability of the daughter cells was lower than that in the control cells [14].

Triptolide (TPL), an active component of the Chinese herb thunder god vine (*Tripterygium wilfordii* Hook. F), was used to treat rheumatoid arthritis and cancer in ancient China [15]. As a broad-spectrum anti-cancer drug, TPL can inhibit ovarian cancer invasion by upregulation of E-cadherin [16], suppress the proliferation of prostate cancer [17] and colon carcinoma together with oxaliplatin [18], and downregulate the ganglioside (GD3) synthase gene expression that contributes to the generation and progression of cancer in human melanoma cells [19] and reverse hypoxia-induced EMT in pancreatic cancer [20].

In this study, TPL was used to treat BT-549 and HEY. Similar to SKOv3 with paclitaxel treatment, the first generation of PGCCs (PGCCs-t) and their daughter cells induced by TPL in BT-549 and HEY cells had lower migration, invasion, and proliferation abilities. As the times of passage increasing, the abilities of migration, invasion, and proliferation of PGCCs-t and their daughter cells gradually enhanced, which may associate with the expression of EMT-related proteins. This transition can be used to mimick that the cancer cells subjected to anti-cancer drugs and acquired strong migration, invasion, and proliferation abilities in the recurrent tumors.

Materials and methods

Cancer cell lines and culture

Human breast cancer line BT-549 and ovarian cancer line HEY were obtained from the American Type Culture Collection (ATCC) (Manassas, VA, USA). Cells were cultured at 37 °C in a humidified atmosphere of 5% CO_2 and maintained in Roswell Park Memorial Institute (RPMI) medium 1640 basic (1×) (Gibco, Norwalk, CT, USA) supplemented with 10% fetal bovine serum (FBS) (Gibco) and 100 U/ml penicillin and 100 µg/ml streptomycin (Gibco).

Formation of PGCCs

When BT-549 and HEY cells reached 80–90% confluence, TPL (Gold WHEAT, Qingpu, Shanghai, China) was added to BT-549 for 48 h and HEY for 9 h at a concentration of 40 ng/ml. After the flask was rinsed with phosphate-buffered saline (PBS) and these cells were cultured in medium without TPL. After two days, most of the regular-sized tumor cells were killed, and only scattered PGCCs survived. Survived PGCCs were cultured in regular medium for 20–30 days, and they began to generate daughter cells. When these cells reached 80–90% confluence, we collected them as first generation cells (P1) and passaged them without TPL until the 5th (P5) and 10th generation (P10). Collected cells were used for western blot and later analyses.

Western blot analysis

The total protein of the control cells, P1, P5 and P10 cells was extracted using radio-immunoprecipitation assay (RIPA) lysis buffer (Thermo Fisher Scientific, Inc.) with 1×Halt Protease & Phosphatase Inhibitor Cocktail (Thermo Fisher Scientific, Inc.). Protein concentrations were determined, and proteins were separated on 6% or 10% sodium dodecyl sulfate (SDS) polyacrylamide gels and transferred to polyvinylidene difluoride (PVDF) membrane (GE, Boston, USA). The membrane was blocked with 5% non-fat dry milk in Tris-buffered saline with 0.1% Tween 20 (TBST) buffer for 2 h at 20–26 °C and incubated with the corresponding antibody with gentle shaking overnight at 4 °C. The membrane was washed three times for 15 min with TBST buffer and then incubated with homologous secondary antibody

and detected using Immobilon Western Chemiluminescent HRP Substrate (Millipore Corporation, Billerica, USA). Images were captured using Bio-Rad imaging system. The densitometric analyses of protein bands were performed using ImageJ software. The antibodies used were the following: rabbit anti-E-cadherin polyclonal (1:2000 dilution; Proteintech, Wuhan, China), rabbit anti-fibronectin polyclonal (1:1000 dilution; ABclonal, Wuhan, China), mouse anti-Twist monoclonal (1:1000 dilution; Novus Biologicals, CO, USA), rabbit anti-vimentin polyclonal (1:2000 dilution; Abcam, Cambridge, UK), mouse anti-β-actin monoclonal (1:1000 dilution; ZSGB-BIO, Xicheng, Peking, China).

Extraction of nuclear and cytoplasmic protein fractions

Nuclear and cytoplasmic protein fractions were prepared using an extraction kit (Beyotime Biotechnology, Shanghai, China) according to the manufacturer's instructions. Simply, the cells were collected and 200 µl of reagent A (containing PMSF) was added into per 20 µl of cell pellets. After full vortex, 10 µl of CER B was added. Immediately, the supernatant (cytoplasmic proteins) was pipetted into a pre-cooling tube for use. The supernatant was thoroughly discarded to avoid contamination of cytoplasmic proteins and 50 µl of NER (containing PMSF) was added to the precipitate. After vortex and centrifuge, the supernatant (nuclear proteins) was immediately taken into a new pre-cooling tube for assay.

Immunocytochemistry (ICC) staining

Cell suspension (100 µl) was placed on sterile coverslips in 6-well plates (Nest, Wuxi, Jiangsu, China). 1.5 ml medium was added into the well and cultured for 2 days in a CO_2 incubator. We performed ICC according to the protocol described by Zhang [6]. Cells were incubated overnight with antibodies including rabbit anti-E-cadherin polyclonal (1:4000 dilution; Proteintech), rabbit anti-fibronectin polyclonal (1:1500 dilution; ABclonal), mouse anti-Twist monoclonal (1:8000 dilution; Novus Biologicals), and rabbit anti-vimentin polyclonal (1:7500 dilution). Finally, the samples were stained with 3,3′-diaminobenzidine (DAB) (ZSGB-BIO) for 15–40 s, counterstained with hematoxylin (Baso, Zhuhai, Guangzhou, China) for 30 s, and washed with running water. Pictures were taken under a microscope (Nikon Eclipse 80i, Japan).

Cell migration and invasion assay

Cells were washed three times with FBS-free medium and counted using an automated cell counter (Invitrogen, CA, USA). For migration and invasion assay, the upper chamber contained 5×10^4 and 5×10^5 cells, respectively. 650 µl of medium containing 10% FBS was added to the lower chamber. Cells were incubated for 20 h in a CO_2 incubator. Then, the medium was removed in the upper and lower chamber and washed with PBS, and cells were fixed in methanol and stained with 0.1% crystal violet. We photographed under a microscope, and cells were counted using ImageJ software.

Wound-healing assay

Cells (1×10^4 per well) were seeded in triplicate onto 6-well plates and cultured for 36–48 h until 95% confluency. The cell monolayers were uniformly scratched using sterile pipette tips. The detached cells were removed by washing with PBS, followed by incubation in serum-free medium. The scratched area between the red-dashed regions was measured by Image-J software. Cells were photographed in marked areas at 0, 12, and 24 h using a microscope. The ability of cell migration was compared by the Wound-Healing Index using the formula described by Fei et al. [10].

Cell counting kit-8 (CCK8) and 3-(4,5-dimethylthiazol-2-yl)-2,5-diphenyltetrazolium bromide (MTT) assay

Cells were collected and counted using an automated cell counter. Then, 2.5×10^3, 5×10^3, and 10×10^3 BT-549 cells and 2×10^3, 4×10^3 and 8×10^3 HEY cells were seeded in a 96-well plate and incubated for 48 h. Then, 10 µl/well CCK-8 (Dojndo, Kumamoto, Japan) and MTT (Solarbo, Tongzhou, Peking, China) were added to 90 µl of medium and incubated for 2 h and 4 h, respectively. After 2 h, CCK8 plates were read using a Bio-Rad microplate reader at wavelength of 450 nm. After 4 h, 110 µl/well formazan dissolved agents were added and shaken in a Micro oscillator for 10 min. MTT plates were read using a microplate reader at a wavelength of 490 nm.

Statistical analysis

All experiments were repeated at least three times. Statistical data were analyzed by statistical software Graphpad Prism 7. All comparisons were performed using Student's *t* test. $P<0.05$ was considered as statistically significant.

Results

TPL induces the formation of PGCCs in breast and ovarian cancers

Breast cancer cell line BT-549 and ovarian cancer cell line HEY were treated with TPL (40 ng/ml) for 48 and 9 h, respectively. The majority of cells were killed, and only

few PGCCs survived. After recover from the TPL treatment, PGCCs can generate daughter cells via budding (Fig. 1A(c–e), B(c–e)). PGCCs with their budding daughter cells were collected as the first generation cells and named as P1 cells (Fig. 1A(c), B(c)), and the 5th and 10th generation cells were collected and named as P5 cells (Fig. 1A(d), B(d)) and P10 cells (Fig. 1A(e), B(e)). The morphology of daughter cells derived from PGCCs after TPL treatment changed from epithelial-like to spindle-like cells. The epithelial and spindle cells co-exist in the same flask following the treatment of TPL. Cells after TPL treatment were all named as PGCCs-t and used for EMT-related protein expression analyses and function experiments.

Different generation PGCCs-t contribute to EMT in breast and ovarian cancers

Because TPL has been reported to reverse hypoxia-induced EMT [20], P1, P5, and P10 generation PGCCs-t and corresponding control cells were collected to study the expression of EMT-related proteins using western blotting and ICC. Compared to the control cells, the total level of E-cadherin decreased significantly in P1, P5, and P10 generation PGCCs-t in BT-549 and HEY cells (Fig. 2A, B(b), C(e–h), D(e–h)). The total and cytoplasmic E-cadherin expression of P10 generation PGCCs-t was higher than that of P5 in HEY cells but still lower than that of the control cells. The nuclear expression of E-cadherin was gradually lower than that of the control cells (Fig. 2A, B(b,h), D(e–h)). The cytoplasmic and P1 nuclear E-cadherin expression had no significantly statistical significance in HEY. In BT-549 cells, the cytoplasmic level of E-cadherin decreased in contrast with that of the control cells, whereas the PGCCs-t had nuclear expression of E-cadherin that gradually increased (Fig. 2A, B(c), C(e–h)) in contrast with HEY cells.

The mesenchymal marker fibronectin level gradually increased in different generation PGCCs-t compared to BT-549 and HEY control cells (Fig. 2A, B(a), C(a–b), D(a–b)). Because of the dynamic expression of fibronectin in different generations, the expression difference between PGCCs-t and control cells gradually enlarged. Based on this, the expression of the P10 generation in BT-549 cells as well as the P5 and P10 generations in HEY cells had a statistical significance. Furthermore, the expression of vimentin, which is also a mesenchymal marker, was notable in our study. Vimentin expression in the P1 and P5 generation PGCCs-t was lower compared to that in the control BT-549 cells, but its expression in the P10 generation was similar to that of the control cells. Thus, P1 and P10 generations did not show statistical significance and the expression of

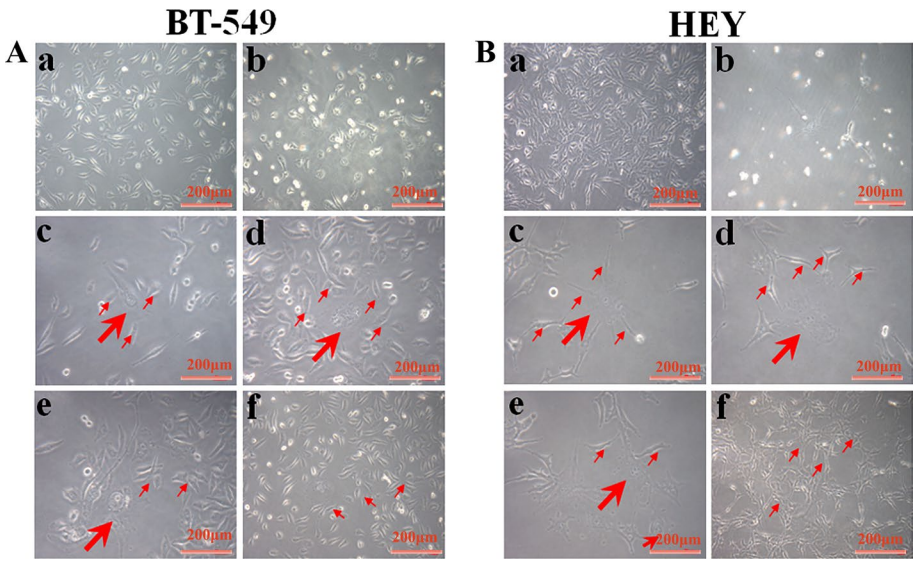

Fig. 1 Triptolide induced the formation of PGCCs. **A** a Control BT-549 cells (100×). b BT-549 cells after TPL treatment for 48 h (100×). c PGCCs generated daughter cells 20–30 days after TPL treatment. Small arrowheads indicate the budding daughter cells in P1 and large arrowhead indicates PGCC in P1 (200×). d Small red arrowheads indicate the budding daughter cells in P5 and large red arrowhead indicates PGCC in P5 (200×). e Small red arrowheads indicate the budding daughter cells in P10 and large red arrowhead indicates PGCC in P10 (200×). f Red arrowheads point the spindle-like daughter cells (100×). **B** a Control HEY cells (100×). b HEY cells after TPL treatment for 9 h (200×). c PGCCs generated daughter cells 20–30 days after TPL treatment. Small red arrowheads indicate the budding daughter cells in P1 and large red arrowhead indicates PGCC in P1 (200×). d Small red arrowheads indicate the budding daughter cells in P5 and large red arrowhead indicates PGCCs in P5 (200×). e Small red arrowheads indicate the budding daughter cells in P10 and large red arrowhead indicates PGCCs in P10 (200×). f Red arrowheads point the spindle-like daughter cells (100×)

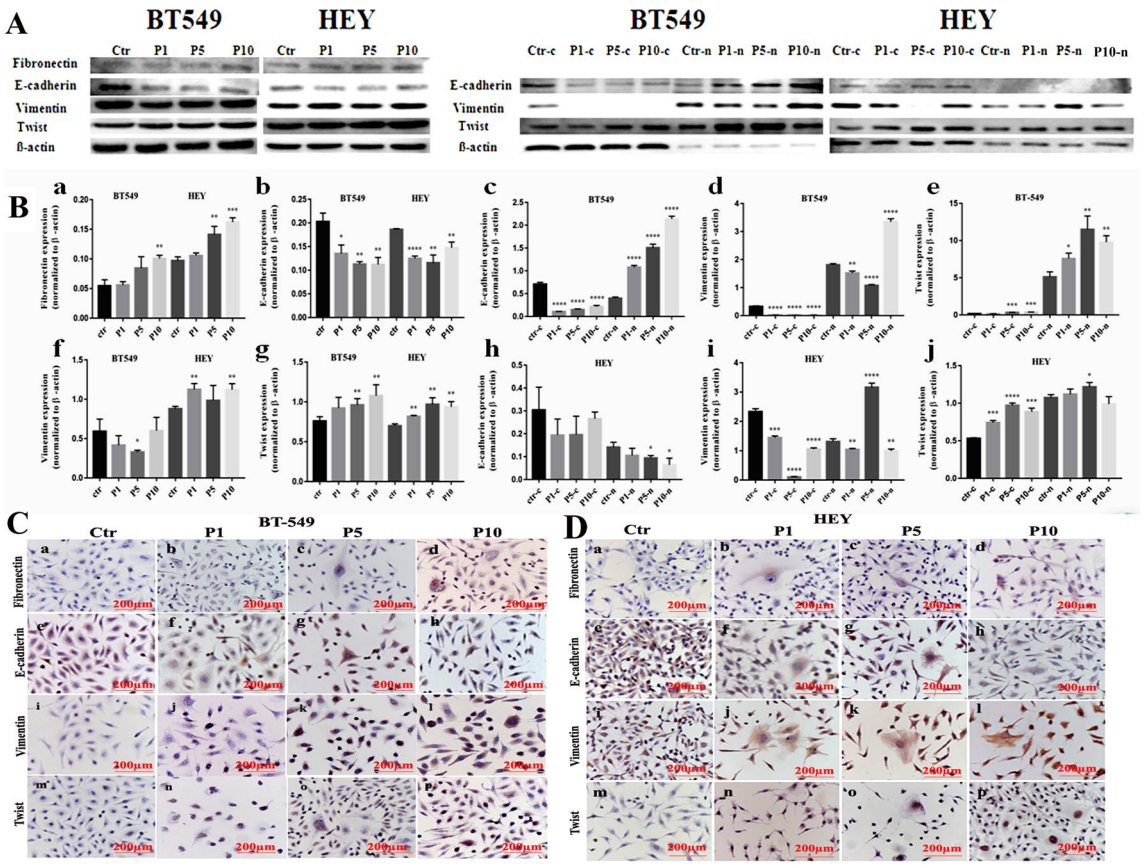

Fig. 2 Western blot analysis showed the expression of fibronectin, E-cadherin, vimentin, and Twist in P1, P5 and P10 PGCCs-t with budding daughter, and control BT-549 and HEY cells. **A** Different expression levels of total proteins, cytoplasmic and nuclear fibronectin, E-cadherin, vimentin, and Twist in P1, P5 and P10 PGCCs-t with budding daughter and control BT-549 and HEY cell. **B** Densitometric analyses of protein bands performed using ImageJ software were normalized to the signal of β-actin. Each bar represents the mean ± standard deviation (SD) of three independent experiments ($^{*}P<0.05$, $^{**}P<0.01$, $^{***}P<0.001$, $^{****}P<0.0001$). **C** ICC staining of E-cadherin, fibronectin, vimentin, and Twist in BT-549 control, P1, P5 and P10 cells (200×). a–d Fibronectin ICC staining in control cells and P1, P5, and P10 cells. e–h E-cadherin ICC staining in control P1, P5, and P10 cells. i–l. Vimentin ICC staining in control, P1, P5, and P10 cells. m–p. Twist ICC staining in control, P1, P5, and P10 cells. **D** ICC staining of E-cadherin, fibronectin, vimentin, and Twist in HEY control, P1, P5 and P10 cells (200×). a–d Fibronectin ICC staining in control, P1, P5, and P10 cells. e–h E-cadherin ICC staining in control, P1, P5, and P10 cells. i–l Vimentin ICC staining in control, P1, P5, and P10 cells. m–p Twist ICC staining in control, P1, P5, and P10 cells

vimentin of PGCCs was located in the nuclear (Fig. 2A, B(d,f), C(i–l)). These data indicated that vimentin expression in different generations of PGCCs-t gradually increased in BT-549 cells. However, in HEY cells, the total level of vimentin in the P1 and P10 generations was higher than that of the controls, and the P5 cells were not obviously differentiated from the control cells, showing no statistical significance (Fig. 2A, B(f,i), D(i–l)).

According to our previous work, Twist had higher expression in PGCCs than that in the control in colorectal cancer [12].Twist played a transcription factor role in EMT to downregulate E-cadherin and claudin expression and upregulate fibronectin and N-cadherin expression [21]. In this study, Twist was overexpressed in cells after TPL treatment compared with the control cells in BT-549 and HEY cells (Fig. 2A, B(g), C(m–p), D(m–p)). In BT-549 cells, Twist expression of PGCCs-t was higher than that of the control cells in the nucleus and cytoplasm. The nuclear Twist was overexpressed in contrast with its cytoplasmic expression and the P5 nuclear expression was the highest (Fig. 2A, B(e), C(m–p)). In HEY cells, the P5 cytoplasmic and nuclear Twist expressions were the highest (Fig. 2A, B(j), D(m–p)).

Different migration and invasion ability of three-generation PGCCs-t

We also examined the migration and invasion ability of P1, P5, and P10 generation PGCCs-t in contrast with control cells. Transwell migration and invasion assays showed that

the number of P1 and P5 generation PGCCs-t were less than those of the control cells, and P10 cells were more abundant than the control cells in BT-549 and HEY cells (Fig. 3A, B). In addition, the wound-healing assay showed similar results to those of the transwell migration assay in HEY cells (Fig. 3D). However, the three-generation PGCCs-t had higher healing abilities compared to the control cells in BT-549 cells (Fig. 3C).

Increased proliferation ability of three-generation PGCCs-t

To examine the proliferation ability of PGCCs-t, we performed CCK8 and MTT assays. The results revealed that the proliferation ability of PGCCs-t gradually increased in P1, P5, and P10 generations, whereas it was low in BT-549 and HEY control cells, except for the 8000-cell group in P10 generation analyzed by MTT assay in HEY cells (Fig. 4A–D).

Discussion

Breast and ovarian cancers are the major threat factors for women health worldwide [1]. Metastasis and relapse of these two cancers aggravate the mortality and decrease the 5-year survival rate. Based on this, it is important to understand the mechanisms of cancer metastasis and relapse. Our previous works reported that $CoCl_2$ [6, 22] and paclitaxel [7] can induce the formation of PGCCs through endoreduplication or cell fusion [11]. PGCCs generate daughter cells via asymmetric division [6], and these daughter cells express low epithelial markers and obtain the mesenchymal phenotype [11], indicating that PGCCs and its daughter cells may be related to the metastasis and relapse of cancer.

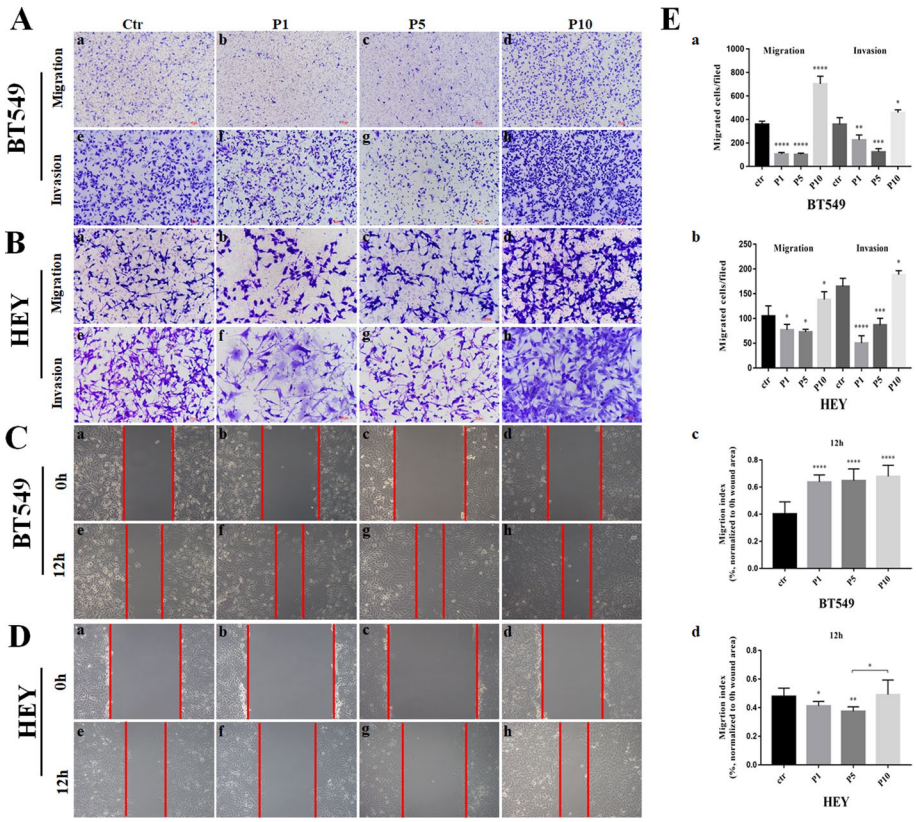

Fig. 3 Transwell migration and invasion assay of BT-549 and HEY control, P1, P5, and P10 cells. **A** Transwell migration and invasion assay in BT-549 cells (100×). a–d Migration ability in control, P1, P5, and P10 cells. e–f Invasion assay of control, P1, P5, and P10 cells. **B** Transwell migration and invasion in HEY cells (200×). a–d Migration ability in control, P1, P5, and P10 cells. e–f Invasion assay of control, P1, P5, and P10 cells. **C** Wound-healing assay was performed for BT-549 cells at 0 and 12 h (100×). a–d Representative images showing the results of wound-healing assay in control, P1, P5, and P10 cells at 0 h. e–f Representative images showing the results of wound-healing assay in control, P1, P5, and P10 cells at 12 h. **D** Wound-healing assay was performed for HEY cells at 0 and 12 h (100×). a–d Representative images showing the results of wound-healing assay in control, P1, P5, and P10 cells at 0 h. e–f Representative images showing the results of wound-healing assay in control, P1, P5, and P10 cells at 12 h. **E** a–d Quantitative results of transwell migration, invasion, and wound-healing assay in BT-549 and HEY cells before and after TPL treatment. Each bar represents the mean ± standard deviation (SD) of three independent experiments ($^{*}P<0.05$, $^{**}P<0.01$, $^{***}P<0.001$, $^{****}P<0.0001$)

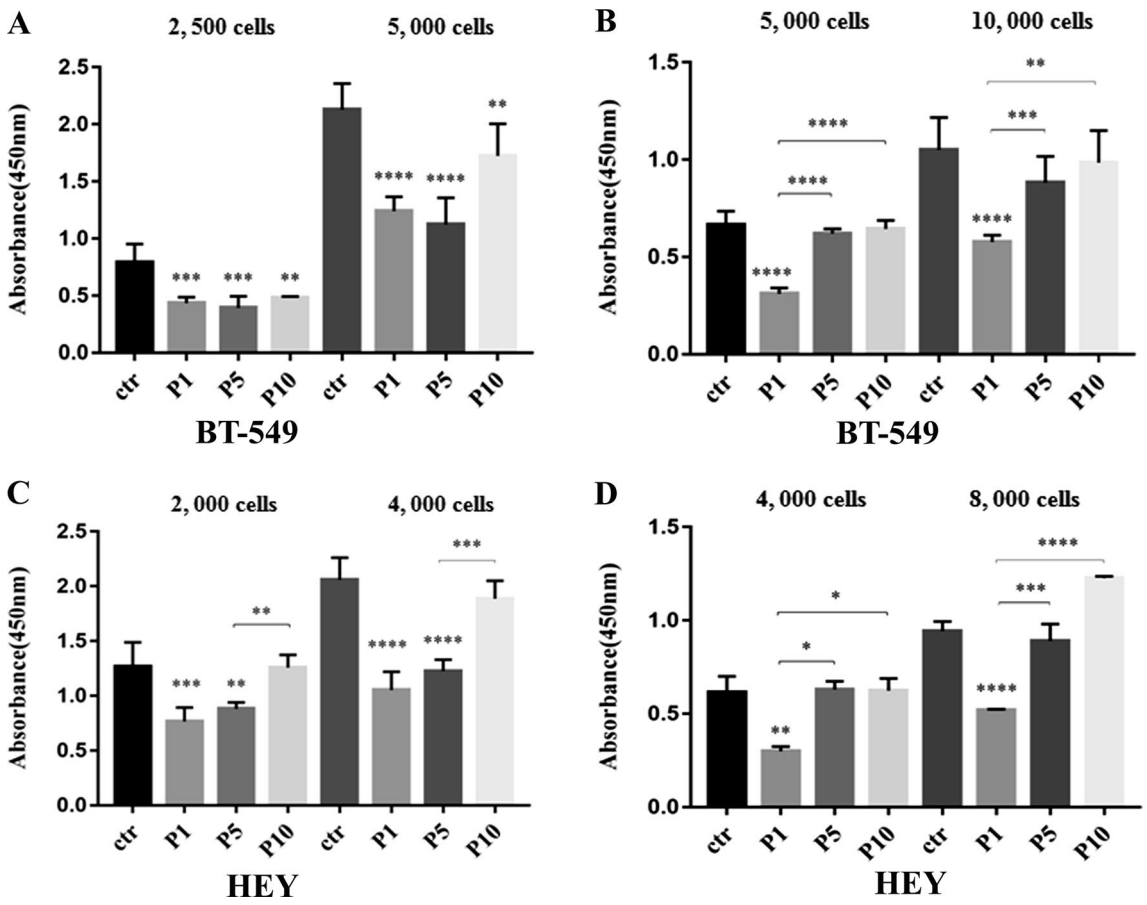

Fig. 4 **A–D**. Comparison of proliferation ability among the control cells (ctr) and P1, P5, and P10 cells in BT-549 and HEY cells was detected by CCK8 and MTT assay at 48 h with different cell numbers. Each bar represents the mean ± standard deviation (SD) of three independent experiments ($^{**}P < 0.01$, $^{***}P < 0.001$, $^{****}P < 0.0001$)

TPL, a diterpenoid epoxide [23], is isolated from Chinese herbal medicine thunder god vine and has anti-inflammatory [24] and anti-cancer effects [16]. In this study, TPL can induce the formation of PGCCs in BT-549 and HEY and these PGCCs can generate daughter cells via asymmetric division. The P1 generation of PGCCs-t, and P5 and P10 generations which were passaged from P1 generation PGCCs-t were used to study the expression of EMT-related proteins including E-cadherin, fibronectin, Twist, and vimentin. EMT can contribute to metastasis and progression of cancer through various cell signaling and organ fibrosis [21, 25, 26]. During EMT, cell morphology exhibits mesenchymal phenotype [21], and upregulation of EMT markers including Twist, fibronectin, and vimentin, as well as downregulation of the E-cadherin [21, 27, 28].

E-cadherin is located in the cell membrane and improves the cell–cell adhesion to inhibit cancer metastasis, acting as a tumor suppressor protein [29]. Low expression of E-cadherin has been reported as a hallmark of EMT and associates with poor prognosis and survival in gastric cancer [30], colon cancer [31], and breast cancer [32]. In addition, the differentially expressed E-cadherin is associated with lymph node metastasis, poor prognosis, and advanced clinical stage in nasopharyngeal carcinoma [33] and lung cancer [34]. Results of our study showed that the total level of E-cadherin in P1, P5, and P10 generation PGCCs-t decreased compared to BT-549 and HEY control cells. Fibronectin is another mesenchymal marker of EMT [35]. In our study, the total level of fibronectin gradually increased in three-generation PGCCs-t in contrast with control cells. Twist also plays a key role in EMT as a transcription factor [21] and associates with poor prognosis in patients with breast cancers [25]. It can decrease the expression of E-cadherin and claudin and increase the expression of fibronectin and N-cadherin [16]. The total expression of Twist in PGCCs-t increased compared to the control cells in this study, which was similar to the expression of fibronectin and E-cadherin. The expression of vimentin is mainly located in cytoplasmic [12]. Aberrant nuclear vimentin contributes to cancer invasion and poor prognosis [33, 36]. In our study, the expression of vimentin is different from that of fibronectin. In BT-549 cells, control cells had higher expression than that of the P1 and

P5 generation PGCCs-t and lower expression compared to P10 generation, and the expression of vimentin in PGCCs-t was located in the nuclear. In HEY cells, the total vimentin expression of P5 generation PGCCs-t was lower than it in P1 and P10 cells, and the P5 generation PGCCs-t is mainly expressed in the nuclear region.

The abilities of proliferation, invasion and migration gradually increased from P1 to P10, and P10 generation of the PGCCs-t had the strongest invasion and migration ability, which showed that the ability to invasive and migrate can gradually increase in PGCCs-t and their daughter cells when they recovered from the treatment of TPL. The proliferation of PGCCs-t was lower than that of the control cells because of the inhibition of TPL and the differences among these three generations of PGCCs-t and control cells gradually decreased, indicating the gradual recovery of proliferative capacity.

In conclusion, we confirmed that TPL induced the formation of PGCCs-t which can produce their daughter cells via asymmetric division. These daughter cells differentially expressed EMT-related properties and the abilities of proliferation, invasion and migration gradually increased. However, the mechanism of nuclear E-cadherin and vimentin expression as well as the shuttling of vimentin between nucleus and cytoplasm should be further explored to identify the mechanism of EMT, which can provide new insights into preventing the metastasis and recurrence of cancer.

Author contributions SZ designed the study; collected, analyzed, and interpreted data; contributed to manuscript writing; and approved the manuscript before submission. XW, FF and CL collected and analyzed data and approved the manuscript before submission. JD and KL collected, analyzed, and interpreted data, contributed to manuscript writing, and approved the manuscript before submission. YL and MZ collected data, gave constructive comments on the manuscript, revised the paper and approved the manuscript before submission.

Funding This work was supported in part by Grants from the National Natural Science Foundation of China (81672426), and the foundation of committee on science and technology of Tianjin (17ZXMFSY00120 and 17YFZCSY00700).

Compliance with ethical standards

Conflict of interest The authors declare that they have no conflict of interest.

References

1. Bray F, Ferlay J, Soerjomataram I, Siegel RL, Torre LA, Jemal A. Global cancer statistics 2018: GLOBOCAN estimates of incidence and mortality worldwide for 36 cancers in 185 countries. CA Cancer J Clin. 2018. https://doi.org/10.3322/caac.21492.
2. Institute NC. SEER cancer statistics review, 1975–2011. Bethesda: National Cancer Institute; 2013.
3. Yeung TL, Leung CS, Yip KP, Au Yeung CL, Wong ST, Mok SC. Cellular and molecular processes in ovarian cancer metastasis. A review in the theme: cell and molecular processes in cancer metastasis. Am J Physiol Cell Physiol. 2015;309(7):C444–56. https://doi.org/10.1152/ajpcell.00188.2015.
4. Scully OJ, Bay BH, Yip G, Yu Y. Breast cancer metastasis. Cancer Genom Proteom. 2012;9(5):311–20.
5. Kozlowski J, Kozlowska A, Kocki J. Breast cancer metastasis - insight into selected molecular mechanisms of the phenomenon. Postepy Hig Med Dosw(Online). 2015;69:447–51.
6. Zhang S, Mercado-Uribe I, Xing Z, Sun B, Kuang J, Liu J. Generation of cancer stem-like cells through formation of polyploid giant cancer cells. Oncogene. 2014. https://doi.org/10.1038/onc.2013.96.
7. Zhang S, Mercado-Uribe I, Liu J. Tumor stroma and differentiated cancer cells can be originated directly from polyploid giant cancer cells induced by paclitaxel. Int J Cancer. 2014;134(3):508–18. https://doi.org/10.1002/ijc.28319.
8. Lv H, Shi Y, Zhang L, Zhang D, Liu G, Yang Z, et al. Polyploid giant cancer cells with budding and the expression of cyclin E, S-phase kinase-associated protein 2, stathmin associated with the grading and metastasis in serous ovarian tumor. BMC Cancer. 2014. https://doi.org/10.1186/1471-2407-14-576.
9. Zhang L, Ding P, Lv H, Zhang D, Liu G, Yang Z, et al. Number of polyploid giant cancer cells and expression of EZH2 are associated with VM formation and tumor grade in human ovarian tumor. Biomed Res Int. 2014. https://doi.org/10.1155/2014/903542.
10. Fei F, Zhang D, Yang Z, Wang S, Wang X, Wu Z, et al. The number of polyploid giant cancer cells and epithelial–mesenchymal transition-related proteins are associated with invasion and metastasis in human breast cancer. J Exp Clin Cancer Res. 2015. https://doi.org/10.1186/s13046-015-0277-8.
11. Zhang S, Zhang D, Yang Z, Zhang X. Tumor budding, micropapillary pattern, and polyploidy giant cancer cells in colorectal cancer: current status and future prospects. Stem Cells Int. 2016. https://doi.org/10.1155/2016/4810734.
12. Zhang D, Yang X, Yang Z, Fei F, Li S, Qu J, et al. Daughter cells and erythroid cells budding from PGCCs and their clinicopathological significances in colorectal cancer. J Cancer. 2017;8(3):469–78. https://doi.org/10.7150/jca.17012.
13. Zhang S, Mercado-Uribe I, Hanash S, Liu J. iTRAQ-based proteomic analysis of polyploid giant cancer cells and budding progeny cells reveals several distinct pathways for ovarian cancer development. PLoS ONE. 2013;8(11):e80120. https://doi.org/10.1371/journal.pone.0080120.
14. Jia L, Zhang S, Ye Y, Li X, Mercado-Uribe I, Bast RC, et al. Paclitaxel inhibits ovarian tumor growth by inducing epithelial cancer cells to benign fibroblast-like cells. Cancer Lett. 2012;326(2):176–82. https://doi.org/10.1016/j.canlet.2012.08.004.
15. Brinker AM, Ma J, Lipsky PE, Raskin I. Medicinal chemistry and pharmacology of genus Tripterygium (Celastraceae). Phytochemistry. 2007;68(6):256. https://doi.org/10.1016/j.phytochem.2006.11.029.
16. Zhao H, Yang Z, Wang X, Zhang X, Wang M, Wang Y, et al. Triptolide inhibits ovarian cancer cell invasion by repression of matrix metalloproteinase 7 and 19 and upregulation of E-cadherin. Exp Mol Med. 2012;44(11):633–41. https://doi.org/10.3858/emm.2012.44.11.072.
17. Han Y, Huang W, Liu J, Liu D, Cui Y, Huang R, et al. Triptolide inhibits the AR signaling pathway to suppress the proliferation of enzalutamide resistant prostate cancer cells. Theranostics. 2017;7(7):1914–27. https://doi.org/10.7150/thno.17852.
18. Liu Y, Xiao E, Yuan L, Li G. Triptolide synergistically enhances antitumor activity of oxaliplatin in colon carcinoma in vitro and in vivo. DNA Cell Biol. 2014;33(7):418–25. https://doi.org/10.1089/dna.2014.2356.

19. Kwon HY, Kim SJ, Kim CH, Son SW, Kim KS, Lee JH, et al. Triptolide downregulates human GD3 synthase (hST8Sia I) gene expression in SK-MEL-2 human melanoma cells. Exp Mol Med. 2010;42(12):849–55. https://doi.org/10.3858/emm.2010.42.12.088.
20. Liu L, Salnikov AV, Bauer N, Aleksandrowicz E, Labsch S, Nwaeburu C, et al. Triptolide reverses hypoxia-induced epithelial–mesenchymal transition and stem-like features in pancreatic cancer by NF-kappaB downregulation. Int J Cancer. 2014;134(10):2489–503. https://doi.org/10.1002/ijc.28583.
21. Lamouille S, Xu J, Derynck R. Molecular mechanisms of epithelial–mesenchymal transition. Nat Rev Mol Cell Biol. 2014;15(3):178–96. https://doi.org/10.1038/nrm3758.
22. Lopez-Sánchez LM, Jimenez C, Valverde A, Hernandez V, Peñarando J, Martinez A, et al. $CoCl_2$, a mimic of hypoxia, induces formation of polyploid giant cells with stem characteristics in colon cancer. PLoS ONE. 2014. https://doi.org/10.1371/journal.pone.0099143.
23. Graziose R, Lila MA, Raskin I. Merging traditional Chinese medicine with modern drug discovery technologies to find novel drugs and functional foods. Curr Drug Discov Technol. 2010;7(1):2–12.
24. Wen HL, Liang ZS, Zhang R, Yang K. Anti-inflammatory effects of triptolide improve left ventricular function in a rat model of diabetic cardiomyopathy. Cardiovasc Diabetol. 2013;12:50. https://doi.org/10.1186/1475-2840-12-50.
25. Zhang YQ, Wei XL, Liang YK, Chen WL, Zhang F, Bai JW, et al. Over-expressed twist associates with markers of epithelial mesenchymal transition and predicts poor prognosis in breast cancers via ERK and Akt activation. PLoS ONE. 2015;10(8):25. https://doi.org/10.1371/journal.pone.0135851.
26. Zhao Z, Lu P, Zhang H, Xu H, Gao N, Li M, et al. Nestin positively regulates the Wnt/β-catenin pathway and the proliferation, survival and invasiveness of breast cancer stem cells. Breast Cancer Res. 2014;16(4):408. https://doi.org/10.1186/s13058-014-0408-8.
27. Jin H, Morohashi S, Sato F, Kudo Y, Akasaka H, Tsutsumi S, et al. Vimentin expression of esophageal squamous cell carcinoma and its aggressive potential for lymph node metastasis. Biomed Res (Tokyo, Japan). 2010;31(2):105–12.
28. Onder TT, Gupta PB, Mani SA, Yang J, Lander ES, Weinberg RA. Loss of E-cadherin promotes metastasis via multiple downstream transcriptional pathways. Cancer Res. 2008;68(10):3645–54. https://doi.org/10.1158/0008-5472.Can-07-2938.
29. Wong SHM, Fang CM, Chuah LH, Leong CO, Ngai SC. E-cadherin: its dysregulation in carcinogenesis and clinical implications. Crit Rev Oncol Hematol. 2018;121:11–22. https://doi.org/10.1016/j.critrevonc.2017.11.010.
30. Xing X, Tang YB, Yuan G, Wang Y, Wang J, Yang Y, et al. The prognostic value of E-cadherin in gastric cancer: a meta-analysis. Int J Cancer. 2013;132(11):2589–96. https://doi.org/10.1002/ijc.27947.
31. Jie D, Zhongmin Z, Guoqing L, Sheng L, Yi Z, Jing W, et al. Positive expression of LSD1 and negative expression of E-cadherin correlate with metastasis and poor prognosis of colon cancer. Dig Dis Sci. 2013;58(6):1581–9. https://doi.org/10.1007/s10620-012-2552-2.
32. Horne HN, Sherman ME, Garcia-Closas M, Pharoah PD, Blows FM, Yang XR, et al. Breast cancer susceptibility risk associations and heterogeneity by E-cadherin tumor tissue expression. Breast Cancer Res Treat. 2014;143(1):181–7. https://doi.org/10.1007/s10549-013-2771-z.
33. Luo W, Fang W, Li S, Yao K. Aberrant expression of nuclear vimentin and related epithelial–mesenchymal transition markers in nasopharyngeal carcinoma. Int J Cancer. 2012;131(8):1863–73. https://doi.org/10.1002/ijc.27467.
34. Deeb G, Wang J, Ramnath N, Slocum HK, Wiseman S, Beck A, et al. Altered E-cadherin and epidermal growth factor receptor expressions are associated with patient survival in lung cancer: a study utilizing high-density tissue microarray and immunohistochemistry. Modern Pathol. 2004;17(4):430–9. https://doi.org/10.1038/modpathol.3800041.
35. Agajanian M, Runa F, Kelber JA. Identification of a PEAK1/ZEB1 signaling axis during TGFbeta/fibronectin-induced EMT in breast cancer. Biochem Biophys Res Commun. 2015;465(3):606–12. https://doi.org/10.1016/j.bbrc.2015.08.071.
36. Liu Z, Kakudo K, Bai Y, Li Y, Ozaki T, Miyauchi A, et al. Loss of cellular polarity/cohesiveness in the invasive front of papillary thyroid carcinoma, a novel predictor for lymph node metastasis; possible morphological indicator of epithelial mesenchymal transition. J Clin Pathol. 2011;64(4):325–9. https://doi.org/10.1136/jcp.2010.083956.